This is a preprint, the final version is subject to change, of the American Mineralogist (MSA)
Cite as Authors (Year) Title. American Mineralogist, in press.
(DOI will not work until issue is live.) DOI: http://dx.doi.org/10.2138/am-2016-5808

Revision 1

Transformation of pyrite to pyrrhotite in the presence of Au-Ag alloys at 500ºC

GALINA PALYANOVA[1,2*], KONSTANTIN KOKH[1,2,3], YURII SERYOTKIN[1,2]

[1]*Sobolev Institute of Geology and Mineralogy, Novosibirsk, Russia*

[2]*Novosibirsk State University, Russia*

[3]*Tomsk State University, Russia*

*Corresponding author: Galina Palyanova

IGM SB RAS, Koptyuga ave., 3, Novosibirsk 630090, Russia, Tel/Fax: +7 383 3066392, E-mail: palyan@igm.nsc.ru

Abstract

Dry annealing of Au_xAg_{1-x} alloys (x=0.19, 0.35, 0.56 or of fineness 300,500,700‰) and pyrite was used to reveal the solubility of Au (Ag) in FeS_2 and study phase equilibria in the FeS_2 - Au_xAg_{1-x} system at 500ºC. Pyrrhotite, acanthite and uytenbogaardtite and Au-Ag alloys with increased fineness were established at the contacts of pyrite blocks with Au-Ag plates. The obtained results evidence the absence of solubility between FeS_2 and Au (Ag) at 500ºC. The Ag content in alloys influences the stability of pyrite and contributes to its transformation in pyrrhotite and sulfidation and ennobling of Au-Ag alloys. Au-Ag sulfides and pyrrhotite may be present in the sulfide ores of metamorphogene deposits as annealing products of Au-Ag-pyrite-bearing ores.

Keywords: desulfidation, pyrite, pyrrhotite, visible and "invisible" gold (silver), isomorphism, thermodiffusion, sulfidation, ennobling of Au-Ag alloys, Au-Ag sulfides

1. Introduction

Pyrite is the most well-known and widespread mineral of the iron sulfides. It is a common constituent of many igneous, metamorphic and sedimentary types of rocks and of hydrothermal

veins. More important is the fact that pyrite is a collector of gold and silver (Boyle 1979; 1980). Revealing the forms of occurrence of noble metals in iron sulfides is of fundamental and applied importance. Pyrite often contains micro inclusions of native gold, Ag-Au chalcogenides and other minerals of gold and silver that are visible under optical microscope and scanning electron microscope (Zhou et al. 2004; Palyanova et al. 2015; 2016). It has been established so far that "invisible" gold occurs as submicron or nano-sized inclusions or solid solution in the structure of iron sulfides (Vikent'ev 2015 and its reference list). The amount of isomorphous gold incorporated into pyrite lattice covers a wide range of values as reported by some authors (Fleischer 1955; Cook and Chryssoulis 1990; Abraitis et al. 2004; Vaughan 2004; Pal'yanova et al. 2015). Gold and silver concentrations in pyrites range from below one ppm to almost thousand ppm.

To determine the probability of incorporation of gold and silver into pyrite, we conducted experiments of solid-phase diffusion (Jin 1981), using natural pure pyrite and synthetic Au-Ag alloys of varying composition. According to this technique, if the plates of two substances A and B are brought into contact and then kept at temperature when diffusion is probable, their composition finally becomes homogeneous. If isomorphism between two components is absent, various compounds stable in the A-B system are formed in the contact zone. This technique is successfully applied to study many binary and ternary systems and construction of the isothermal sections of phase diagrams (Kodentsov et al. 2001). However, this technique has restrictions – melting should be avoided. Data from the phase diagram Fe-S (Kullerud and Yoder 1959; Arnold 1962; Waldner and Pelton 2005; Wang and Salveson 2005) evidence that pyrite is unstable at temperatures above 742-745ºC and melts incongruently with formation of pyrrhotite and sulfur. At temperatures between the melting point and 325ºC, pyrite coexists with pyrrhotite of various compositions $Fe_{1-y}S$ ($0.78<y<1$) or FeS_x ($1< x<1.23$). To avoid melting of pyrite, the specified temperature in the experiments was 500ºC. Application of this technique allows studying phase equilibria in the FeS_2 - Au_xAg_{1-x} system. One of the tasks of the investigation was

to study the behavior of noble metals in the process of desulfidation of pyrite (Craig andVokes 1993; Thomas et al. 2011) and sulfidation of native gold (Pal'yanova et al. 2014), which are typical of natural processes.

2. Experiments and analytical methods

2.1. Starting compositions

In the experiments we used a large natural pyrite single crystal from the Berezovskoe gold-quartz deposit (Ural, Russia). Microprobe analysis showed that pyrite crystal is homogeneous and does not contain micro impurities. First, a plate ~5-6 mm thick was cut from the crystal. After polishing on 1 μm diamond paste, the plate was cut into bars with polished area ~3x3 mm. Gold-silver alloys of $Au_{0.19}Ag_{0.81}$, $Au_{0.35}Ag_{0.65}$ and $Au_{0.56}Ag_{0.44}$ composition (gold fineness = 1000·Au/(Au+Ag), by weight, 300, 500 and 700‰, respectively) synthesized from a stoichiometric mixture of pure metals were rolled out to the thickness of ~200 micron and cut into plates measuring 3x3 mm. Then metal sheets were placed between polished surfaces of the pyrite bars, and the resulting column was sealed under 10^{-3} torr in the quartz ampoule. The samples were slowly heated to 500ºC in the isothermal zone of the furnace and kept at this temperature for 7 days. After annealing, the ampoule was cooled to room temperature in the switched off furnace.

2.2. Analytical techniques

Optical microscopy, scanning electron microscopy (SEM), electron microprobe analysis (EPMA) and X-ray powder diffraction methods were applied to study the samples. A polished section was prepared from the synthesized phases for microscopy analyses. Studies on the chemical composition of the synthesized substances were carried out using MIRA 3 LMU SEM (TESCAN Ltd.) combined with the microanalysis system INCA Energy 450+ on the basis of the high sensitive silicon drift detector XMax-80, and WDS INCA Wave 500 (Oxford Instruments

Ltd.). The analyses were conducted at 20 kV accelerating voltage, 1.5 nA probe current. Most analyses of Au-Ag sulfides were performed using SEM-EDS at 15–20 s live acquisition time of spectrum. Acquisition of spectra was performed in the raster mode with the scanning area from 0.5 × 0.5 μm^2 for fine phases, and to 2 × 2 μm^2 for larger phases with a slightly defocused electron beam. While a bulk composition of decay structures was obtained with the scanning area from 5×5 μm^2 to 10 × 10 μm^2. The analyses were made with a slightly defocused electron beam, to reduce the destructive effects of the electron beam on unstable Au-Ag sulfides. For analysis we used the characteristic X-ray S K-series and L-series of Ag and Au. Under these conditions the random error of measurement caused by the counting statistic for Au-Ag sulfide, corresponding to uytenbogaardtite was 0.17, 0.37, and 0.98 wt.% for S, Ag, and Au, respectively. Detailed measurement techniques have been worked out for the natural Au-Ag sulfides and described in (Pal'yanova et al. 2014). Pure silver and gold, PbS and $CuFeS_2$ were used as standards for Ag, Au, S, and Fe, respectively.

X-ray powder diffraction study of the synthesized phases was performed on a Stoe IPDS-2T diffractometer (MoKα radiation, graphite monochromator) using Gandolfi mode. Two-dimensional X-ray patterns were radially integrated using the XArea software package. The diffraction profiles were treated by using the WinXPow (Stoe) program packages. For the phase analysis, the database of PDF-4 Minerals (The Powder Diffraction File PDF-4 +, 2006) was used.

3. Results

The data on solid phase products of experiments are given in Table 1. The reaction zones between pyrite blocks and Au-Ag alloys contained pyrrhotite, acanthite- and uytenbogaardtite phases and Au-Ag alloys of fineness higher than the initial fineness, but lower than 830‰ (Figs.1, 2). It was established that pyrrhotite in all three zones had an identical and stable composition very close to Fe_7S_8. Analysis of Au-Ag alloys shows up to 1.6 weight % of sulfur,

105 which may be explained by micro inclusions of Au-Ag sulfides. The fineness of alloys was
106 calculated without account of sulfur. Acanthite and uytenbogaardtite form the structures of solid
107 solution decay. SEM photos made at high magnification (Fig. 3a-c) show two phases of Au-Ag
108 sulfides well discriminated by color - acanthite (light grey) and uytenbogaardtite (grey). It is
109 supposed that this aggregate reflects the possible composition of the Au-A sulfide solid solution
110 stable at 500°C.

111 The amount of acanthite phase prevails in all experiments. According to EPM analysis,
112 the mole ratios of metals to sulfur (Ag+Au)/S in the acanthite and uytenbogaardtite phases vary
113 from 1.5 to 1.6, which is considerably lower compared to their ideal compositions. This may be
114 described by the visually observed partial decomposition of the phases under ion beam. The
115 features of phases and chemical compositions of each reaction zone are described below:

116 **Pyrite + Ag-Au alloy (300‰):** In the reaction zone with initial low-fineness alloy we
117 established alloys with the fineness from 830 near the pyrite to 740‰ in the middle part of the
118 alloy plate (Figs.1a, 2a, 4a, Table 1). Uytenbogaardtite forms parallel thin veinlets (less than 1-3
119 micron wide) in acanthite (Fig. 3a). The maximal content of gold reaches 29.4 wt.% in
120 uytenbogaardtite ($Ag_{2.98}Au_{0.84}S_2$). Acanthite was analyzed as $Ag_{>1.61-1.54}S$. The possible bulk
121 composition of the Au-Ag sulfide solid solution existing at 500°C corresponds to the formula
122 $Ag_{1.60}Au_{0.26}S$.

123 **Pyrite + Ag-Au alloy (500‰):** In the reaction zone with the initial alloyof medium
124 fineness we have established alloys of fineness from 520 to 830‰ (Fig.1b,2b, Table 1).In
125 contrast to previous sample, the fineness of alloy has varied more slightly remaining almost
126 unchanged in the center (Fig. 4b). Gold content does not exceed 8 wt.% in Au-Ag sulfides. Au-
127 Ag sulfides are presented by two phases (Fig. 3b) – acanthite ($Ag_{1.60}Au_{0.05}S$) and
128 uytenbogaardtite ($Ag_{3.26}Au_{0.50}S$). The possible composition of Au-Ag sulfide solid solution
129 stable at 500°C is equal to $Ag_{1.62}Au_{0.06}S$ (Table 1).

130 **Pyrite + Ag-Au alloy (700‰):** The alloy of a high-fineness appeared to be most stable.
131 The reaction zone in this experiment (Figs.1c, 2c) is narrower than those with alloys of fineness
132 300 (Figs.1a, 2a) and 500‰ (Figs.1b, 2b). Purely unreacted areas of the alloy were found in the
133 central parts. The maximum fineness of the reacted alloy, again, does not exceed 830‰. The
134 fineness of alloys insignificantly increased from the center of the Au-Ag plate toward the contact
135 with pyrite (Fig.2c, 4c). In Au-Ag sulfides, gold concentration varies from 1.1 to 8.2 wt.%. Two
136 phases of Au-Ag sulfides were found - acanthite ($Ag_{1.50}Au_{0.01}S$) and uytenbogaardtite
137 ($Ag_{3.12}Au_{0.17}S_2$). The possible bulk composition of the Au-Ag sulfide stable at 500°C is equal to
138 $Ag_{1.55}Au_{0.03}S$ (Table 1).

139 Figure 4 shows the variations of Fe, S, Au and Ag concentrations along the reaction
140 zones and new phases found between pyrite and Au-Ag alloys in each experiment. The same
141 pattern of variations in Fe and S concentrations was established in all samples. The concentration
142 of sulfur decreases in transition from pyrite to pyrrhotite and further to Au-Ag sulfides. Finally,
143 its content becomes almost zero in Au-Ag alloys. Iron has the same behavior; its concentration
144 falls to zero in Au-Ag alloys and Au-Ag sulfides. The alloy plates have considerable variation of
145 Au/Ag ratio and the most constant composition was found in the sample with initial 300 ‰
146 fineness. A similar pattern of noble metals redistribution was found in each experiment (Fig.4a-
147 c). Au content close to the contact with pyrite is maximal and appears to be higher than that in
148 the initial alloy. While silver concentration is lower than in initial alloy and it gradually increases
149 towards the center of alloy plate.

150 The estimations of the composition of sulfide solid solution at 500°C showed that the
151 maximum content of Au belongs to the sample with 300‰ plate. Impurities of noble metals were
152 not found in pyrite and pyrrhotite or their content was lower than the detection limit of EPMA.

153 Figure 5 demonstrates redistribution of elements throughout the reaction zone formed at
154 the contact of the 500‰-fineness alloy and pyrite. Compared to gold (Fig. 5b), the silver (Fig.
155 5a) is more intensively transferred from Au-Ag alloys to react with sulfur, which appeared as a

result of pyrite desulfidation. The final products of reaction at 500°C are Au-Ag sulfide solid solution, which decomposes at room temperature, and pyrrhotite Fe_7S_8 substituting pyrite (Fig. 5c).

X-ray powder diffraction results show that pyrite, pyrrhotite, acanthite, uytenbogaardtite, and Au-Ag alloys are present in each reaction zone (Fig. 6). In all samples the peaks intensities of uytenbogaardtite phase are considerably lower than those of acanthite phase, which is confirmed by EPMA analyses (Fig.3a-c).

4. Discussion

Data from Lambert et al. (1998) evidence that thermal decomposition of pyrite in the temperature range of 347-700°C in vacuum proceeds with the formation of pyrrhotite and a gas phase that mainly consists of S_2:

$$FeS_2 = FeS_x + 0.5(2-x)S_2(g)\ 1<x<1.23 \quad (1),$$

And pyrrhotite composition is determined by the equation: $x=1.45\cdot10^{-4}\cdot T(K)+1.0354$. The composition of pyrrhotite calculated by this equation is 1.147, which is in good agreement with the data of microprobe analysis of pyrrhotite from the reaction zones (Fe_7S_8~$FeS_{1.14}$).

According to data of electrum-tarnish method (Barton and Toulmin 1964), at 500°C in the presence of pyrite-pyrrhotite buffer the alloys of fineness lower 780‰ must be sulfidated and become black. In our experiments all three alloys have turned black due to sulfidation which agrees with the previous data. In addition, we have found newly formed uytenbogaardtite and Au-enriched noble alloys. Francis (1971) investigated the kinetics and mechanism of electrum tarnish by sulfur. One of his results was a decrease of silver in Au-Ag alloys put in contact with silver sulfide.

Since pyrite blocks and Au-Ag plates were placed into one ampoule, the value of sulfur pressure was identical for all samples and was mainly determined by the pyrite-pyrrhotite buffer at 500°C, and probably by some average activity of gold and silver in alloy plates.

Pyrite desulfidation is accompanied by a sulfidation reaction of Au-Ag alloys. According to the solid state products found in the reaction zones, the following quazi-reaction is assumed to take place between pyrite and Au-Ag alloys (in general mode):

$7FeS_2 + aAu_xAg_{1-x} \rightarrow Fe_7S_8 + 6Ag_{2-y}Au_yS + cAu_zAg_{1-z}$ ($0<x<1$, $0<y<1.1$, $x<z<1$, $a>12$, $c>0$) (2).

The ternary $Ag_{2-y}Au_yS$ sulfides lie from Ag_2S to slightly beyond AgAuS (Barton 1980). From eq. (2) it is possible to estimate the compositions of Au-Ag sulfide solid solution. Table 1 contains the calculated variations in the solid solution according to the measured range of Au-Ag alloys in each sample. It may be concluded that the sample with 300‰ alloy is mostly close to the equilibrium since the EPMA data of Au-Ag sulfide solid solution decay structures have shown the highest content of gold. Also, the fineness of resulting alloy has the shortest range 740-830 ‰ compared to 510-830 and 700-830 ‰ intervals found in the experiments with 500 and 700 ‰ initial alloys, respectively.

Au-Ag sulfide solid solution is unstable at room temperature and therefore it decomposes to form a mixture of acanthite and uytenbogaardtite or uytenbogaardtite and petrovskaite, according to Ag_2S – Au_2S phase diagram (Folmer et al. 1976; Barton 1980; Osadchii and Rappo 2004; Palyanova et al. 2011). When studying the system Fe-Au-S, it was impossible to synthesize Au_2S by a similar reaction with gold even at high temperatures and longer period of time (Barton and Toulmin 1964; Toulmin and Barton 1964). In the system Fe-Ag-Au-S we obtained Ag-Au sulfides of various compositions through melt crystallization: Ag_2S, Ag_3AuS_2, AgAuS and solid solutions $(Ag,Au)_2S$ together with pyrite and pyrrhotite (Palyanova et al. 2012).

The sulfidation reactions of native gold with participation of S_2 gas were considered in a few papers (Barton et al. 1978; Barton 1980; Gurevich et al. 2011; Palyanova et al. 2014). These reactions may provide one or two phases of Au-Ag sulfides and ennobled alloys up to pure gold (Palyanova et al. 2014). The results of this work also evidence that sulfidation of Au-Ag alloys

proceeds through a quazi-equilibria resulting in the formation of alloy with a higher fineness according to reaction (2).

The pyrite, close to or at a distance from the reaction zone, and the newly formed pyrrhotite contain no traces of gold and silver. It is worth noting that pyrite which was not at the contact with Au-Ag plates did not undergo any changes. These data suggest that gold and silver do not dissolve in pyrite and are not incorporated isomorphously into its structure.

It was established before that pyrite stability is controlled partly by temperature and pressure, and partly by the amount of H_2O (Tomkins 2010). Our results suggest that in a dry system the presence of silver in the initial alloys seems to promote the reactions of desulfidation of pyrite and sulfidation of Ag-Au alloys. Interestingly that the lower the fineness of initial alloys, the higher is the rate of desulfidation reaction of pyrite and parallel sulfidation reaction of Au-Ag alloys. In natural processes, pyrite containing micro inclusions of native gold on heating will react with them to form pyrrhotite Fe_7S_8 and Au-Ag sulfides (acanthite, uytenbogaardtite and petrovskaite) and higher fineness Au-Ag alloys. The presence of native gold inclusions, especially low fineness, in pyrite will promote pyrrhotite formation.

5. Implications

A great number of gold deposits are characterized by the presence of visible inclusions of native gold in pyrite and in the intergrain space of pyrite (Zhou et al. 2004). We predict the presence of Au-Ag sulfides with pyrrhotite for metamorphogene deposits with native silver, kustelite, electrum and pyrite. Au-rich native gold is stable and less disposed to sulfidation in comparison to the Ag-rich alloys. Sulfidation reactions of native gold with the appearance of Au-Ag sulfides - acanthite, uytenbogaardtite, petrovskaite, or their mixtures (such as acanthite with uytenbogaardtite or uytenbogaardtite with petrovskaite) are typical of some gold deposits (Palyanova et al. 2014; 2016). Au-Ag sulfides in association with pyrite and Fe-sphalerite were found in several mines: Konechnoe Au–quartz occurrence (Taimyr, Russia) (Proskurnin et al.

233 2011); Au–Ag deposits - Broken Hills adularia-sericite (Hauraki Goldfield, New Zealand)
234 (Cocker et al. 2012) and Dzhulietta (northeastern Russia) (Palyanova et al. 2016). The number
235 of deposits with uytenbogaardtite with petrovskaiteis is increasing every year
236 (http://www.mindat.org/min-4127.html).

237 Along with a hypergeneous origin and crystallization from hydrothermal solutions,
238 volcanic gases or sulfide melts (Cocker et al. 2012; Palyanova et al. 2011; 2012; Savva et al.
239 2012), these Au-Ag sulfides could be formed due to sulfidation of Au-Ag alloys in
240 metamorphogene processes. According to the relationship between the fineness of alloy and the
241 rate of pyrite/alloy reaction, the amount of resulting acanthite should prevail that of
242 uytenbogaardtite and petrovskaite.

243 In the annealing products of Au-Ag-pyrite-bearing ores the presence of Au-Ag sulfides and
244 pyrrhotite is also probable. The higher mobility of silver compared to gold during
245 thermodiffusion at the contact of Au-Ag alloys with pyrite is one of the probable mechanisms of
246 the increase in gold fineness and genesis of Au-Ag sulfides in nature. The presence of fine-
247 grained micro inclusions of Au-Ag sulfides, which are hard to diagnose in pyrite-bearing ores,
248 can be one of the reasons for the low extracting ability of noble metals.

249

250 **Acknowledgments**

251 This work is supported by the Russian Foundation for Basic Research, grant N 14-05-00504a.
252 The authors thank Dr. Khokhryakov A.F. which gave us a pyrite crystal for research. We thank
253 Dr. N.S. Karmanov (Institute of Geology and Mineralogy SB RAS) for the electron microprobe
254 studies of polished sections and Dr. V.V. Bakakin (Institute of Inorganic Chemistry SB RAS) for
255 advice. We are sincerely thankful to the Editor Prof. Foustoukos and anonymous reviewer for
256 their comments and constructive suggestions which improved this manuscript.

257

258 **References cited:**

Abraitis, P.K., Pattrick, R.A.D., and Vaughan, D.J. (2004) Variations in the compositional, textural and electrical properties of natural pyrite: a review. International Journal of Mineral Processing, 74, 41–59.

Arnold, R.G. (1962) Equilibrium relations between pyrrhotite and pyrite from 325° to 741°C. Economic Geology, 57, 72–90.

Barton, M.D. (1980) The Ag-Au-S system. Economic Geology, 75, 303–316.

Barton, P.B. Jr., and Toulmin, P. (1964) The electrum-tarnish method for the determination of the fugacity of sulfur in laboratory sulfide systems. Geochimica et Cosmochimica Acta, 28, 619–640.

Boyle, R.W. (1968) The geochemistry of silver and its deposits. Geological Survey of Canada, Ottawa.

Boyle, R.W. (1979) The Geochemistry of Gold and Its Deposits. Geological Survey of Canada, Ottawa.

Chareev, D.A., and Osadchii, E.G. (2006) Thermodynamic studies of pyrrhotite–pyrite equilibria in the Ag–Fe–S system by solid-state galvanic cell technique at 518–723 K and total pressure of 1 atm. Geochimica et Cosmochimica Acta, 70, 5617–5633.

Cocker, H.A., Mauk, J.L., Rabone, S.D.C., 2013. The origin of Ag–Au–S–Se minerals in adularia-sericite epithermal deposits: constraints from the Broken Hills deposit, Hauraki Goldfield, New Zealand. Miner. Deposita 48 (2), 249–266.

Cook, N.J., and Chryssoulis, S.L., (1990) Concentrations of “invisible gold” in the common sulfides. Canadian Mineralogist, 28, 1–16.

Craig, J. R., and Vokes, F.M. (1993) The metamorphism of pyrite and pyritic ores: an overview. Mineralogical Magazine, 57, 3–18.

Fleischer, M. (1955) Minor elements in some sulphide minerals. Economic Geology 50th Anniv. V., 970–1024.

284 Folmer, J.C.W., Hofman, P., and Wiegers, G.A. (1976) Order-disorder transitions in the system
285 $Ag_{2-x}Au_xS$ ($0 < x < 1$). J. Less-Common Metals, 48, 251–268.
286 Francis, D.M. (1971) Electrum-tarnish by sulfur: a study of an irreversible processes. A thesis of
287 Degree Master of Science. The University of British Columbia. 58p.
288 Jin, Z. (1981) A Study of the Range of Stability of Phase in Some Ternary Systems.
289 Scandinavian Journal of Metallurgy, 10, 279–287.
290 Kodentsov, A.A., Bastin, G.F., and Loo, van F.J.J. (2001) The diffusion couple technique in
291 phase diagram determination. Journal of Alloys and Compounds, 320, 207–217.
292 Kullerud, G., Yoder, H.S. (1959) Pyrite stability relations in the Fe-S system. Economic
293 Geology, 54, 533–572.
294 Lambert, J.M., Simkovich, J.R., and Walker, P.L. (1998) The kinetics and mechanism of the
295 pyrite-to-pyrrhotite transformation. Metallurgical and Materials Transactions B, 29B, 385–
296 396.
297 Pal'yanova, G.A., Kravtsova, R.G., Zhuravkova, T.V. (2015) $Ag_2(S,Se)$ solid solutions in the
298 ores of the Rogovik gold-silver deposit (northeastern Russia). Russian Geology and
299 Geophysics, 56, 1738–1748.
300 Pal'yanova, G., Mikhlin, Yu., Kokh, K., Karmanov, N., and Seryotkin, Yu. (2015) Experimental
301 constraints on gold and silver solubility in iron sulfides. Journal of Alloys and Compounds,
302 649, 67-75.
303 Palyanova, G., Karmanov, N., and Savva, N. (2014) Sulfidation of native gold. American
304 Mineralogist, 99, 1095-1103.
305 Palyanova, G.A., Kokh, K.A., and Seryotkin, Yu.V. (2012) Formation of gold-silver sulfides and
306 native gold in Fe-Ag-Au-S system. Russian Geology and Geophysics, 53, 321-329.
307 Palyanova G.A., Savva N.E., Zhuravkova T.V., E.E. Kolova. (2016) Gold and silver minerals in
308 low-sulfide ores of the Dzhulietta deposit (*northeastern Russia*) // Russian Geology and
309 Geophysics, 57, 1171–1190.

Proskurnin, V.F., Palyanova, G.A., Karmanov, N.S., Bagaeva, A.A., Gavrish, A.V., 2011. The first discovery of uytenbogaardtite in Taimyr (Konechnoe occurrence). Dokl. Earth Sci. 441 (2), 1661–1665.

Taylor, L.A. (1970) The system Ag-Fe-S: phase equilibria and mineral assemblages. Mineral. Deposita, 5, 41–58.

The Powder Diffraction File PDF-4+, International Centre for Diffraction Data (ICDD), Release, 2006.

Thomas, H.V., Large, R.R., Bull, S.W., Maslennikov, V.V., Berry, R.F., Fraser, R., Froud, S., and Moye, R. (2011) Pyrite and Pyrrhotite textures and composition in sediments, laminated quartz veins, and reefs at Bendigo Gold Mine, Australia: Insights for ore genesis. Economic Geology, 106, 1-31.

Tomkins, A.G. (2010) Windows of metamorphic sulfur liberation in the crust: Implications for gold deposit genesis. Geochimica et Cosmochimica Acta, 74, 3246–3259.

Toulmin, P., and Barton, P.B. Jr. (1964) A thermodynamic study of pyrite and pyrrhotite. Geochimica et Cosmochimica Acta, 28, 641–671.

Vaughan, J.P. (2004) The process mineralogy of gold: the classification of ore types. Journal of metals, 56, 46–48.

Vikentyev, I.V. (2015) Invisible and microscopic gold in pyrite: methods and new data for massive sulfide ores of the Urals. Geology of Ore Deposits, 57, 237–265.

Waldner, P., and Pelton, A.D. (2005) Thermodynamic modeling of the Fe-S system. Journal of Phase Equilibria and Diffusion, 26, 23-38.

Wang, H., and Salveson, I. (2005) A review on the mineral chemistry of the non-stoichiometric iron sulphide, $Fe_{1-x}S$ ($0 \leq x \leq 0.125$): polymorphs, phase relations and transitions, electronic and magnetic structures. Phase Transitions, 78, 547–567.

White, J.L., Orr, R.L., and Hultgren, R. (1957) Thermodynamic properties of silver–gold alloys. Acta Metallurgica, 5, 747–760.

Zhou, J., Jago, B., and Martin, C. (2004-03) Establishing the process mineralogy of gold ores. SGS Miner. Tech. Bull., 1–16.

http://www.mindat.org/min-4127.html

Figure captions

Figure 1. Photo (in reflected light) of polished sections: phases in the reaction zone formed at the contact of pyrite and Au-Ag alloys of fineness 300 (a), 500 (b) and 700 ‰ (c). Symbols of the phases: Py – pyrite, Po – pyrrhotite, Ac – acanthite, Uy – uytenbogaardtite, N_{Au} – fineness of Au-Ag alloys, ‰.

Figure 2. SEM photo of phases in the reaction zone formed at the contact of pyrite and Au-Ag alloys of fineness 300 (a), 500 (b) and 700 ‰ (c).

Figure 3. SEM photo of Au-Ag sulfides (acanthite and uytenbogaardtite phases) formed at the contact of pyrite and Au-Ag alloys of fineness 300 (a), 500 (b) and 700 ‰ (c) as well as their relationships and compositions.

Figure 4. Cross-section showing the content of elements (in wt.%) and phases along the "reaction zones" between pyrite and Au-Ag alloys of fineness 300 (a), 500 (b) and 700 ‰(c).

Figure 5. Distribution of elements Ag (a), Au (b), Fe (c) and S (d) in characteristic radiations (AgLα1, AuMα1, FeKα1, SKα1, respectively) over the scanning area of reaction zone formed at the contact of pyrite and alloy of fineness 500‰.

Figure 6. X-ray powder diffraction pattern of sample with 700‰ initial alloy. Vertical lines under graph represents the peaks position of (from top to bottom): experimental pattern, gold, uytenbogaardtite Ag_3AuS_2, pyrite FeS_2, pyrrhotite Fe_7S_8 and acanthite Ag_2S.

Table 1. Initial fineness (N_{Au}) and compositions of Au-Ag alloys and compositions of new phases formed at the contact Au-Ag alloys and pyrite at 500°C.

№	Initial Au-Ag alloys (N_{Au})	Compositions of new phases				
		Au-Ag alloys (N_{Au}‰)	Au-Ag sulfides 25°C	Au-Ag sulfide ss 500°C[1]	Au-Ag sulfide ss (reaction 2)[2]	Iron sulfide
1	$Au_{0.19}Ag_{0.81}$ (300)	$Au_{0.61}Ag_{0.39}$ (740) $Au_{0.72}Ag_{0.28}$ (830)	Ac ($Ag_{>1.54\text{-}1.61}S$) Uy ($Ag_{2.98}Au_{0.84}S_2$)	$Ag_{1.60}Au_{0.26}S$	$Ag_{1.69}Au_{0.31}S$ $Ag_{1.71}Au_{0.29}S$	$Fe_{0.875}S$
2	$Au_{0.35}Ag_{0.65}$ (500)	$Au_{0.36}Ag_{0.64}$ (510) $Au_{0.73}Ag_{0.27}$ (830)	Ac ($Ag_{1.60}Au_{0.05}S$) Uy ($Ag_{3.26}Au_{0.50}S_2$)	$Ag_{1.62}Au_{0.06}S$	$Ag_{1.30}Au_{0.70}S$ $Ag_{1.36}Au_{0.64}S$	$Fe_{0.875}S$
3	$Au_{0.56}Ag_{0.44}$ (700)	$Au_{0.56}Ag_{0.44}$ (700) $Au_{0.73}Ag_{0.27}$ (830)	Ac ($Ag_{1.50}Au_{0.01}S$) Uy ($Ag_{3.12}Au_{0.17}S_2$)	$Ag_{1.55}Au_{0.03}S$	- $Ag_{1.28}Au_{0.72}S$	$Fe_{0.875}S$

[1] compositions of acanthite-uytenbogaardtite mixture, obtained with the scanning extended area with a slightly defocused electron beam at EPMA;

[2] calculated compositions of the solid sulfide solutions on reaction 2 for a=13 and c=1 according to the measured range of Au-Ag alloys in each sample (column 3 left)

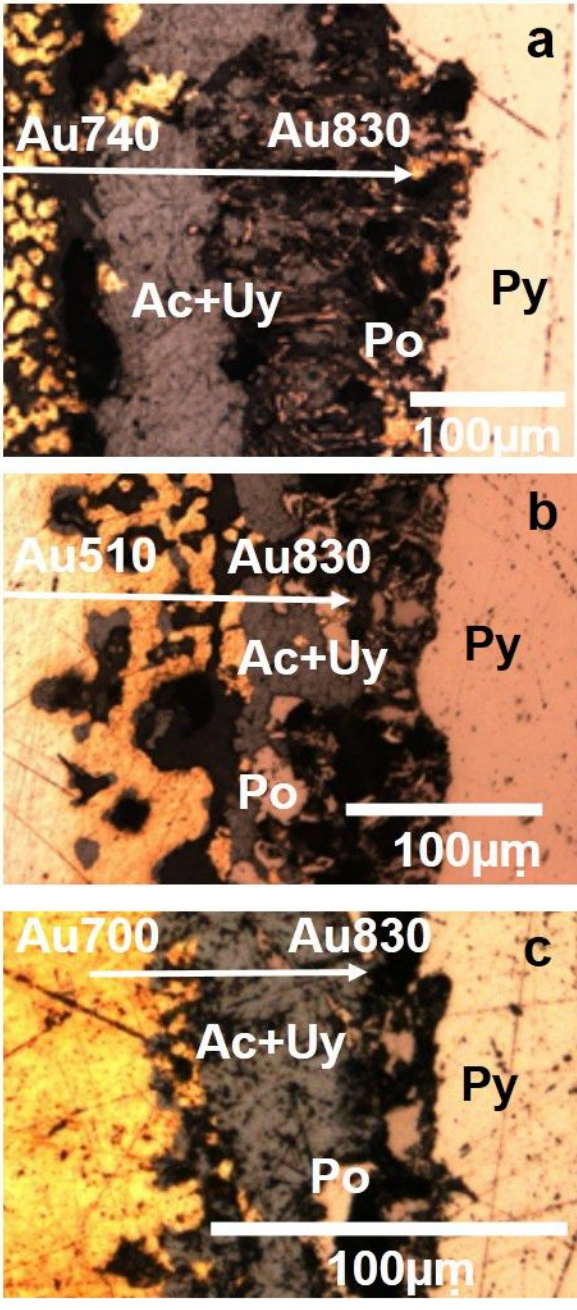
a
Au740
Au830
Ac+Uy
Py
Po
100µm
b
Au510
Au830
Ac+Uy
Py
Po
100µm
c
Au700
Au830
Ac+Uy
Py
Po
100µm

Figure 1.

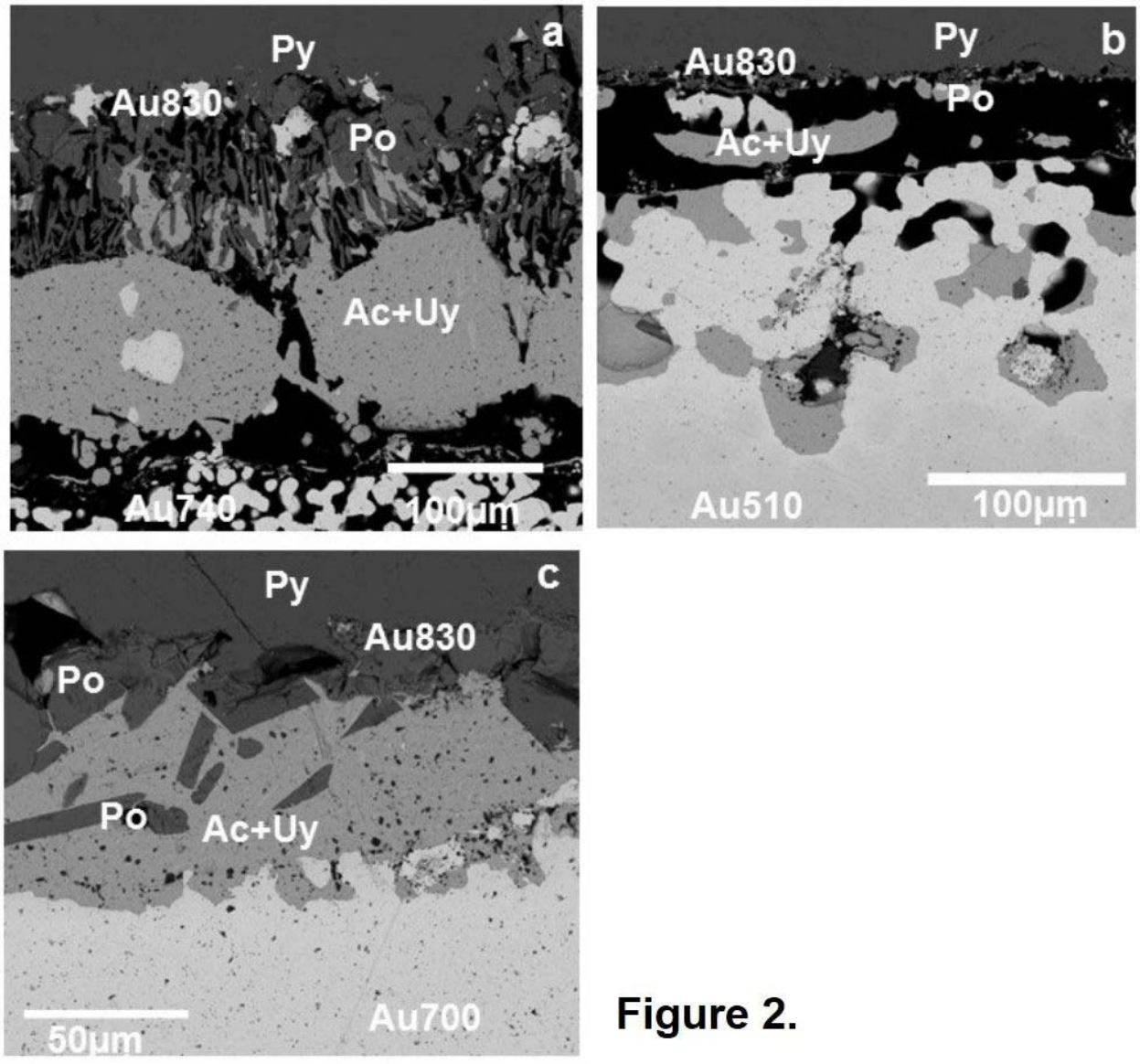
a
Py
Au830
Po
Ac+Uy
Au740
100μm
b
Au830
Py
Po
Ac+Uy
Au510
100μm
c
Py
Au830
Po
Po
Ac+Uy
50μm
Au700

Figure 2.

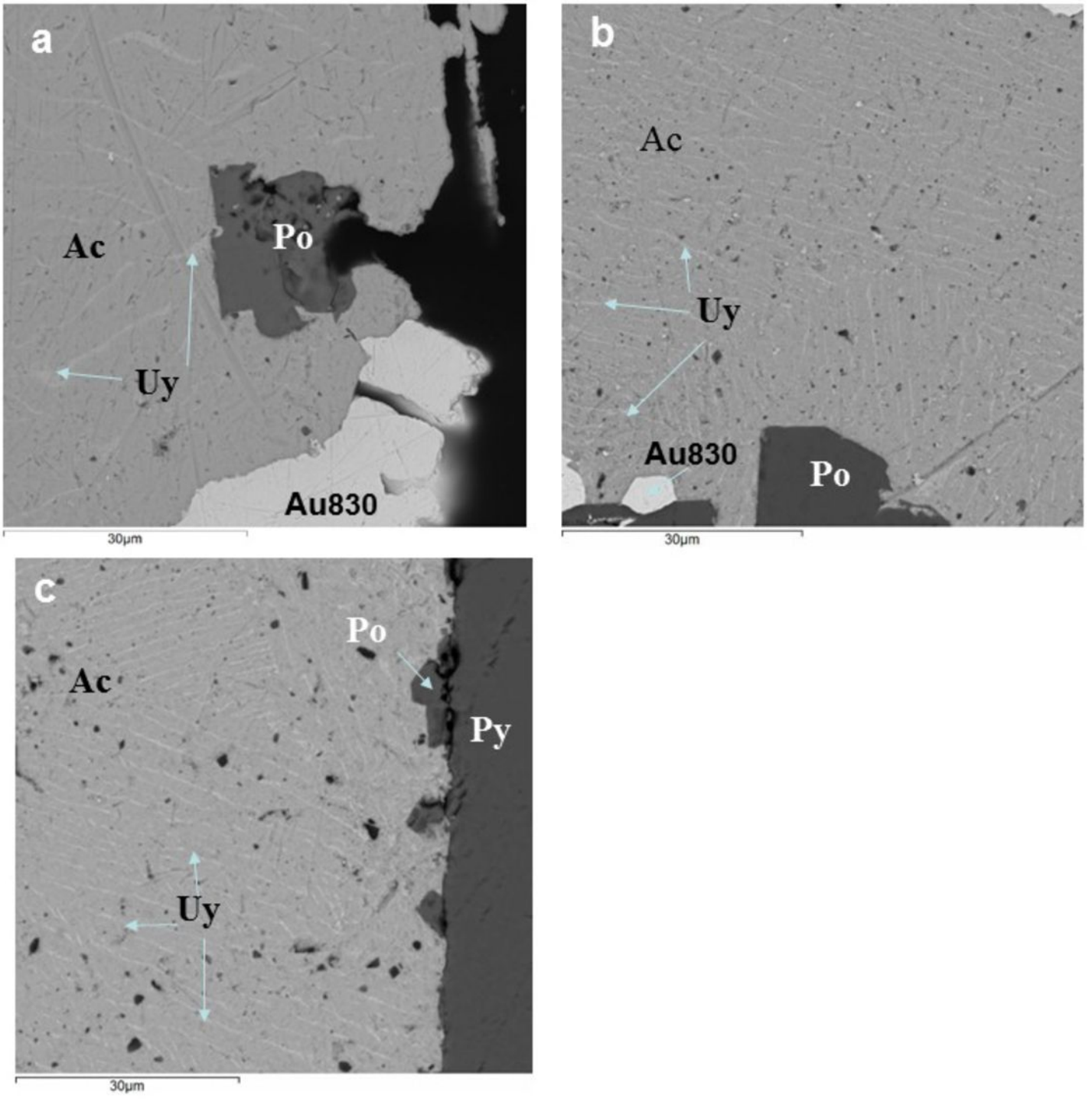

Figure 3.

Figure.4

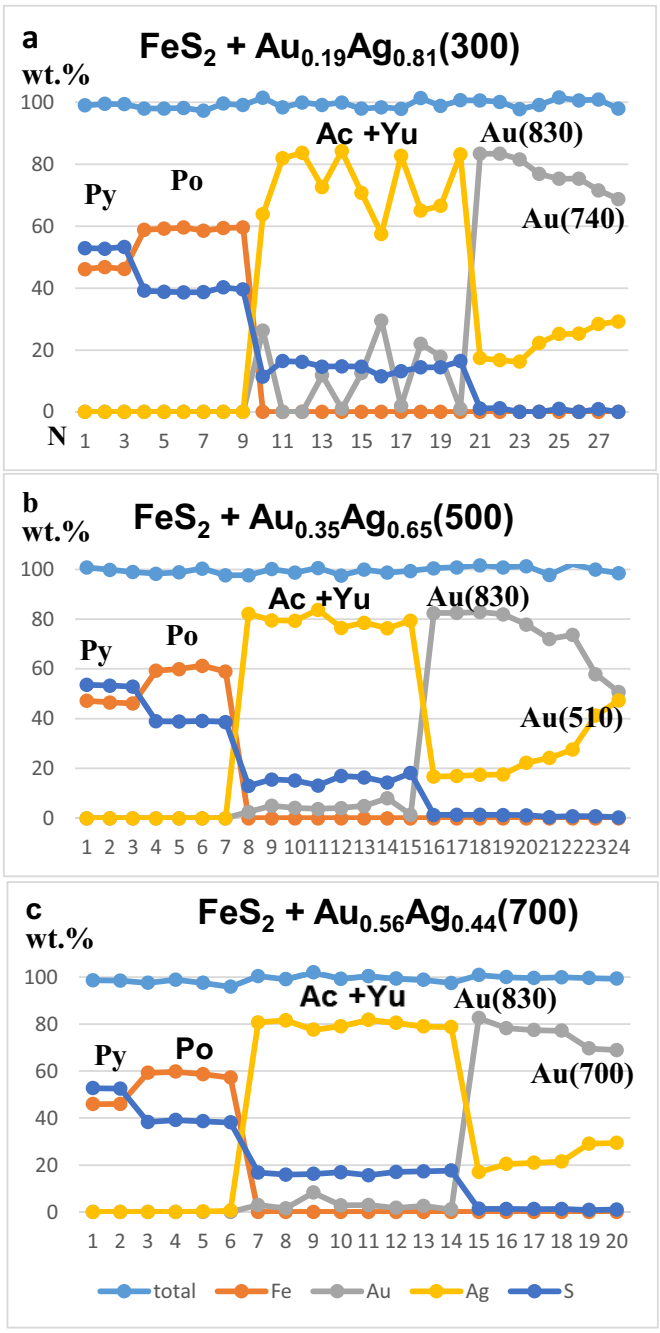
a
wt.%
FeS2 + Au0.19Ag0.81(300)
Py
Po
Ac +Yu
Au(830)
Au(740)
N
b
wt.%
FeS2 + Au0.35Ag0.65(500)
Py
Po
Ac +Yu
Au(830)
Au(510)
c
wt.%
FeS2 + Au0.56Ag0.44(700)
Py
Po
Ac +Yu
Au(830)
Au(700)
total
Fe
Au
Ag
S

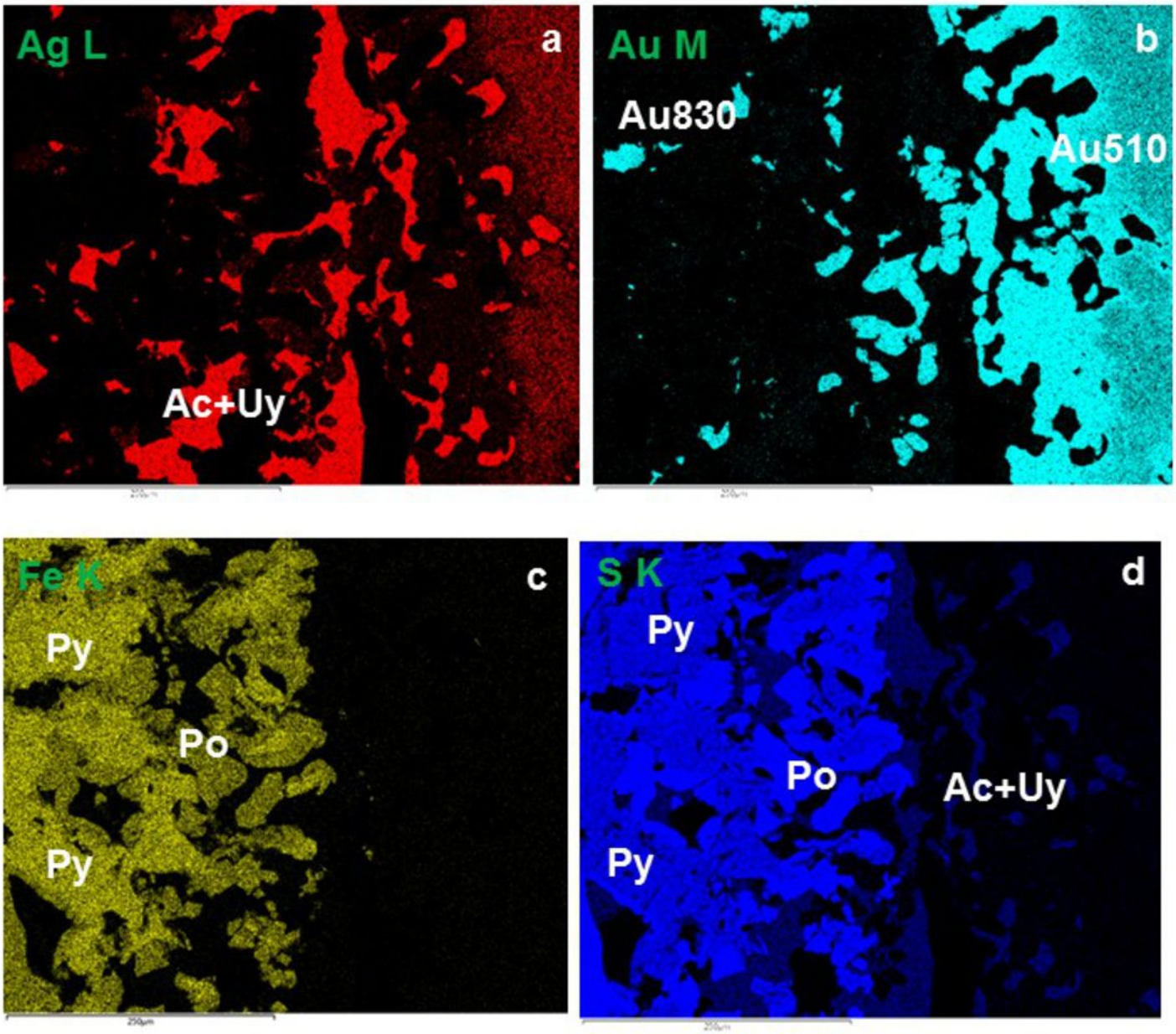

Figure 5

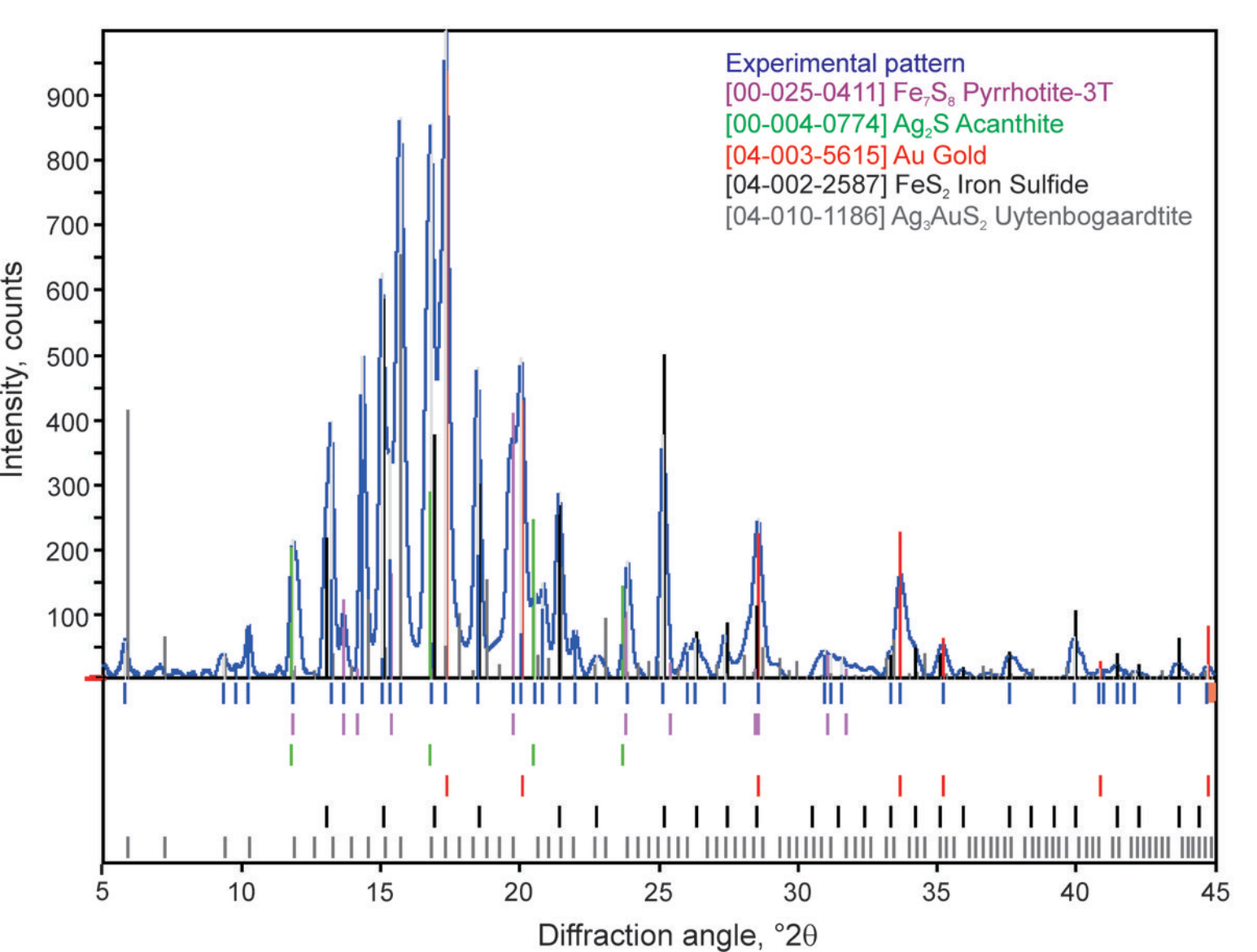
Experimental pattern
[00-025-0411] Fe_7S_8 Pyrrhotite-3T
[00-004-0774] Ag_2S Acanthite
[04-003-5615] Au Gold
[04-002-2587] FeS_2 Iron Sulfide
[04-010-1186] Ag_3AuS_2 Uytenbogaardtite
Intensity, counts
100
200
300
400
500
600
700
800
900
5
10
15
20
25
30
35
40
45
Diffraction angle, °2θ